

Simultaneous Reduction of Fuel Consumption and NO_x Emissions through Hybridization of a Long Haulage Truck

Olov Holmer Lars Eriksson

Vehicular Systems, Dept. Electrical Engineering, Linköping University, SE-58183 Linköping, Sweden (e-mail: {olov.holmer, lars.eriksson}@liu.se).

Abstract: Hybridization is a promising and obvious way of reducing fuel consumption in automotive applications, however, its ability to reduce emissions in long haulage trucks is not so obvious. The complexity of the powertrain is also increased which makes well designed control systems needed to fully utilize the potential benefits of the hybridization. In this paper, a control strategy that takes advantage of the complex structure of the powertrain in a hybrid electric long haulage truck is developed and evaluated. The control system is based on equivalent consumption minimization strategy where an equivalence factor is used to compare fuel and battery power so that an optimal distribution of power between the components in the powertrain can be calculated. The proposed control system is evaluated in a driving scenario using a model of a complete hybrid electric truck, including an aftertreatment system, and the results are compared with a conventional, non-hybrid, vehicle. The hybridization leads to 31 % lower NO_x emissions, primarily due to better thermal conditions in the exhaust system during braking, and at the same time, the fuel consumption was reduced by 3.8 % compared to the non-hybrid vehicle.

© 2017, IFAC (International Federation of Automatic Control) Hosting by Elsevier Ltd. All rights reserved.

Keywords: Hybrid Electric Truck, Automotive Emissions, Powertrain Control, Aftertreatment System, Energy Management, Optimal Control

1. INTRODUCTION

To meet the demand for more fuel efficient vehicles and at the same time keep emissions within the legislated limits, the powertrain in modern vehicles have become complex systems. For example, in heavy-duty applications a fuel efficient engine in combination with an aftertreatment system consisting of particulate filters and catalysts are now standard. Another trend is electrification and hybridization of conventional engine-based powertrains. Hybrid electric vehicles have shown capability of improving fuel economy compared to conventional, non-hybrid, vehicles Chan (2007), so also for the specific case of long haulage trucks Hellström et al. (2010). However, the effect on emissions are not so straightforward since engine-out emissions can increase as a result of changed operation points of the engine CARB (2015). But by shifting the operating point of the engine to an operation point with higher exhaust temperatures the efficiency of the aftertreatment system can be increased during low load conditions Foster et al. (2008) and Willems and Foster (2009). Emissions can also be reduced as a direct result of less power being produced by the engine Willems and Foster (2009). However, to fully make use of all the benefits of hybrid powertrains, well designed control strategies are needed.

In this paper a control strategy for a hybrid electric vehicle based on the Equivalent Consumption Minimization Strategy (ECMS), that takes advantage of the complex structure of the powertrain to simultaneously reduce fuel consumption and NO_x emissions, is developed. For the

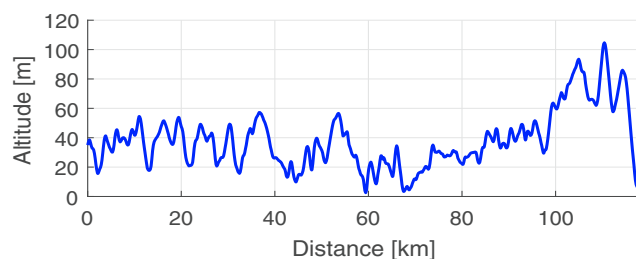


Fig. 1. Altitude profile of the road used to evaluate the proposed control system.

aftertreatment system to be efficient the temperature is important, therefore control strategies that explicitly considers the thermal state of the hybrid vehicle have been developed, for example Willems et al. (2011) and Lescot et al. (2010). Here the thermal effects are not explicitly considered, but still the fuel efficient use of the electrified driveline have shown to keep temperatures in the aftertreatment system at good levels. The control strategy is evaluated by comparing it with a non-hybrid vehicle in the scenario described below.

1.1 Scenario Definition

The scenario used to evaluate the control strategy is defined as a driving mission where the truck should drive the approximately 120 km long Swedish E4 highway from Södertälje to Norrköping with a given mean velocity and payload. The altitude profile of the road is shown in Fig. 1.

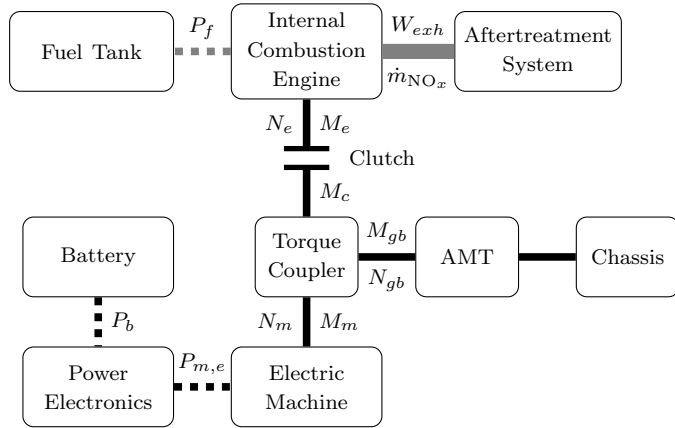


Fig. 2. Configuration of the hybrid vehicle.

1.2 Contributions

The main contribution is the investigation of how the aftertreatment system in a long haulage truck is affected by a hybridization of the truck, in particular, how the SCR temperatures are affected.

2. VEHICLE MODEL

In this section models for two vehicles are presented, one is a hybrid vehicle and the other one is a non-hybrid vehicle. The same engine and aftertreatment system is used in both vehicles, and the components are designed to comply with the Euro VI emissions regulation.

The hybrid vehicle is a parallel hybrid electric vehicle with the configuration shown in Fig. 2. The model is based on Eriksson et al. (2016), and all components are the same as in the above mentioned paper except for the engine which has been modified slightly. The model also include some new components, namely: an aftertreatment system, a torque coupler, a battery, power electronics, and an electric motor. All the modifications and new components are explained below.

The non-hybrid vehicle is also based on Eriksson et al. (2016), and uses the same modification of the engine and addition of an aftertreatment system as the hybrid vehicle.

2.1 Internal Combustion Engine and Clutch

The internal combustion engine is a 12.7 litre, 400 hp diesel engine developed in Wahlström and Eriksson (2011). This model is extended with maps for engine out NO and NO₂ mass flows \dot{m}_{NO} and \dot{m}_{NO_2} , respectively. The maps are two-dimensional and depend on engine torque M_e and speed N_e .

To be able to decouple the engine from the rest of the driveline, during gearshifts or to reduce friction when only the electric motor is used, a clutch is placed between the engine and the torque coupler. The clutch can either be slipping or locked. During clutch slip the engine can rotate independently from the rest of the driveline and when the clutch is locked the two systems rotate with identical speed. For more information about the clutch, see Eriksson (2001).

2.2 Aftertreatment System

The aftertreatment system consists of a Diesel Oxidation Catalyst (DOC), a Diesel Particulate Filter (DPF) and a urea-based Selective Catalytic Reduction (SCR) system.

The SCR catalyst is a 22 litre Cu-Zeolite catalyst and is modeled using a one-dimensional model where the catalyst has been split lengthwise into five segments. In each segment the temperature, reactions, and pressure drop are modeled in a similar way as in Winkler et al. (2003) and Van Helden et al. (2004).

The models for the DPF and DOC are similar to that of the SCR catalyst. However, in the DPF no reactions or soot load build up is modeled and the reactions in the DOC is calculated using maps. The maps for the DOC calculate NO_x after the DOC based on NO_x before the DOC, temperature of the DOC and space velocity, SV , defined as

$$SV = 36000 \frac{W_{exh}}{\rho_{exh} V_{DOC}} \quad (1)$$

where ρ_{exh} is exhaust gas density during normal operation and V_{DOC} is the volume of the DOC.

2.3 Battery

The battery model is based on a Thévelin equivalence circuit with an open circuit voltage, U_{oc} , that depends on the state of charge, SOC , and internal resistance R_i . The battery current, I_b , is calculated as

$$I_b = \frac{U_{oc}(SOC)}{2R_i} - \sqrt{\frac{U_{oc}(SOC)^2}{4R_i^2} - \frac{P_b}{R_i}} \quad (2)$$

where P_b is the terminal power of the battery. The dynamics of the SOC is

$$\dot{SOC} = -\frac{I_b}{Q_0} \quad (3)$$

where Q_0 is the capacity of the battery. Finally, the electrochemical power, P_{ech} , is given by

$$P_{ech} = I_b U_{oc}(SOC). \quad (4)$$

The modelled battery has a capacity of 15.5 kWh and was dimensioned to match the power requirement from the electric motor in the admissible operation range of the battery. The parameters for the battery is taken from XALT Energy (2016).

2.4 Electric Motor and Power Electronics

The model for the electric motor is a static map-based model that also includes the losses in the power electronics. The control signal for the motor, u_m , is the electric power from the power electronics, $P_{m,e}$, i.e. $u_b = P_{m,e}$. Since the losses in the power electronics are lumped into the model for the motor, the power electronics can be considered to be ideal, so that

$$P_b = P_{em,e}. \quad (5)$$

The torque produced by the motor, M_m , is calculated from a map based on $P_{em,e}$ and the speed of the electric motor N_m .

The modelled motor has a rated torque and power of 1000 Nm and 120 kW, respectively, and the map of the

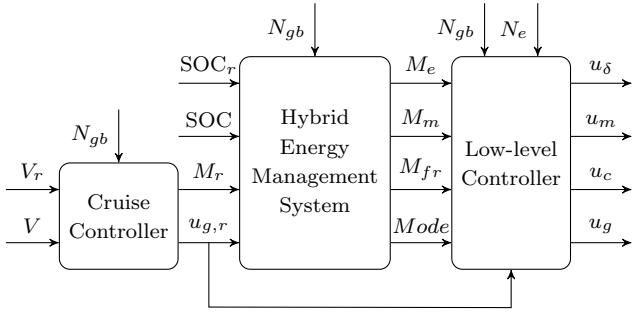


Fig. 3. Schematic overview of the controller for the hybrid vehicle.

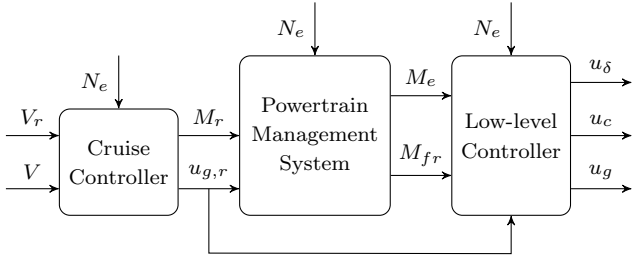


Fig. 4. Schematic overview of the controller for the non-hybrid vehicle.

motor has been produced by a motor design tool developed in Le Berr et al. (2012).

2.5 Torque Coupler

The torque coupler connects the engine and motor with the automated manual transmission (AMT). Since the maximum speed of the motor is higher than that of the engine there is a gear with gear ratio γ_{tc} in the torque coupler to match the speed of the motor, N_m , and engine, N_e . When the clutch is locked N_e is identical to the speed of the input shaft of the AMT, N_{gb} , and we get the following

$$N_{gb} = N_e = \frac{1}{\gamma_{tc}} N_m. \quad (6)$$

The torque on the input shaft of the AMT, M_{gb} , is calculated as

$$M_{gb} = M_c + \gamma_{tc} M_m \quad (7)$$

where M_c is the torque transmitted through the clutch.

3. CONTROLLER

The controllers for both vehicles consist of three parts: a cruise controller that calculates the required torque needed to follow the reference speed, an energy management system that decides how the required torque should be split between the different torque generating components in the powertrain, and a low-level controller that controls the specific control signals for each component in the powertrain. The structure of the controller for the hybrid and non-hybrid vehicles are shown in Fig. 3 and Fig. 4, respectively.

3.1 Cruise Controller

The cruise controller calculates a requested torque at the wheels, M_r , and a gear request, $u_{g,r}$, based on the reference velocity, V_r , the velocity of the vehicle, V , and N_{gb} .

To calculate M_r a proportional controller is used:

$$M_r = K_p(V_r - V) \quad (8)$$

where the feedback gain K_p was tuned to give a stationary error of 1 km/h when a constant reference speed of 80 km/h was used on a flat road.

The gear request is based on N_{gb} in the following way: if $N_{gb} < 900$ RPM a downshift is made, if $N_{gb} > 1250$ RPM an upshift is made, and if $N_{gb} > 1800$ RPM a double upshift is made.

3.2 Hybrid Energy Management System

The main purpose of the hybrid energy management system (HEMS) is to decide how M_r should be split between M_e , M_m , and the friction brake torque, M_b . It also decides which of the following modes should be used:

Mode 1: Both the engine and motor are connected to the AMT.

Mode 2: The engine is turned off and decoupled, and only the motor is connected to the AMT.

To do this, map-based ECMS, based on Sivertsson et al. (2011), is used. ECMS, as first proposed in Brahma et al. (2000) and Paganelli et al. (2000), uses an equivalence factor, λ , to compare fuel power, P_f , and electrochemical power, P_{ech} , when deciding how the torque should be distributed. The problem can be formulated as

$$H = P_f + \lambda P_{ech} \quad (9)$$

$$[M_e, M_m, M_{fr}, Mode] = \text{argmin } H \quad (10)$$

subject to:

$$(M_e + \gamma_{tc} M_m + M_{fr}) \gamma_{gb} = \bar{M}_r \quad (11)$$

$$M_{e,min}(N_e) \leq M_e \leq M_{e,max}(N_e) \quad (12)$$

$$M_{m,min}(N_m) \leq M_m \leq M_{m,max}(N_m) \quad (13)$$

$$M_{fr,min} \leq M_{fr} \leq 0 \quad (14)$$

where $M_{i,min}$ and $M_{i,max}$ denotes the minimum and maximum torque, respectively, for component $i \in [e, m, b]$ and \bar{M}_r is the torque closest to M_r that is possible to produce without violating any of the conditions (12)-(14).

In the map-based ECMS, the solution to (10) is calculated offline for different values on M_r , N_{gb} , and λ creating a three-dimensional map of optimal values of M_e , M_m , M_{fr} and $Mode$ for different operating points. This map can then be used online in an efficient way.

Under the assumption that the battery efficiency is independent of SOC, the equivalence factor λ remains approximately constant along the optimal trajectory Sivertsson et al. (2011). However, if the future driving conditions are unknown, there are no way of knowing the optimal λ . Therefore, an adaptive estimation of λ is used. The adaption is given by

$$\lambda = \lambda_c + K_\lambda \tan\left(\frac{\pi}{2dSOC}(SOC - SOC_r)\right) \quad (15)$$

where λ_c is the value that the adaption is centered around, K_λ is a constant that control the slope of the adaption, SOC_r is the reference SOC, and $dSOC$ is the allowed deviation from SOC_r . The variables λ_c and K_λ was chosen as the values that gave the best fuel economy after iteratively testing different values. The chosen values are $\lambda_c = 2.8$ and $K_\lambda = 0.65$.

In order to avoid frequent engine starts/stops two thresholds are used, $t_{on/off}$ and t_{mode} . The first threshold says that the controller has to request a mode change for a duration longer than $t_{on/off} = 2$ s for the mode change to take place and the other one prevents the controller from changing mode before $t_{mode} = 15$ s have past since the last mode change. The values of $t_{on/off}$ and t_{mode} were found heuristically by testing different values and choosing the values that gave the best performance.

3.3 Powertrain Management System (non-hybrid)

The powertrain management system for the non-hybrid vehicle decides how M_r is split between M_e and M_{fr} . The most fuel efficient way of doing this is to avoid using the friction brakes except when it is necessary, this gives the following control strategy:

$$M_e = \begin{cases} M_{e,max}(N_e), & M_r > M_{e,max}(N_e) \\ M_r, & M_{e,min}(N_e) \leq M_r \leq M_{e,max}(N_e) \\ M_{e,min}(N_e), & M_r < M_{e,min}(N_e) \end{cases} \quad (16)$$

and

$$M_{fr} = \begin{cases} 0, & M_r \geq M_{e,min}(N_e) \\ M_r - M_{e,min}(N_e), & M_r < M_{e,min}(N_e) \end{cases} \quad (17)$$

3.4 Low-level Controller

In the low-level controller the control signals from high-level controllers are translated to control signals for the different components in the vehicle.

For the engine, M_e is translated into injected amount of fuel, u_δ , using a map of the engine. The other control signals to the engine are kept constant, the VGT opening is kept at 60 % and the EGR valve at 0 %. For more information about the different control signals for the engine, see Wahlström and Eriksson (2011).

In a similar way as for the engine, M_m is translated to u_m using a map of the motor.

In mode 1 gear changes are done in the same ways as in Eriksson et al. (2016), with the addition that also the motor torque is ramped up and down during the gear change. In mode 2 the clutch is opened to decouple the engine, and therefore only the motor has to be controlled during gear changes.

3.5 Urea Dosing Controller

The urea dosing controller controls the flow of AdBlue into the exhaust system. The controller consists of a PID controller that tries to minimize the difference between the stored ammonia in the SCR catalyst and its reference, θ_{ref} . The reference for the stored ammonia varies with the temperature of the SCR catalyst and was calibrated to keep the average and peak ammonia slip within 10 and 25 [ppm], respectively, during the driving mission defined in Section 1.1. The same controller was used in both the hybrid and non-hybrid, and in Fig. 5 the used reference is shown.

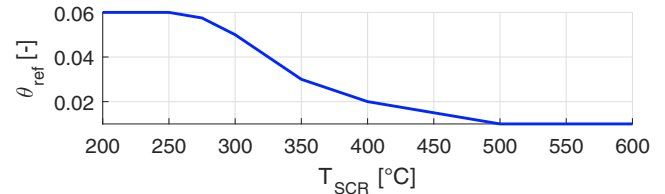


Fig. 5. Reference ammonia storage.

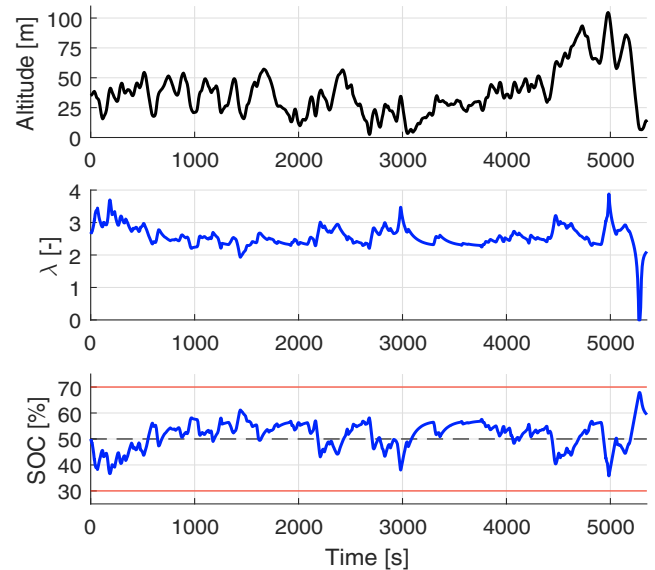


Fig. 6. Altitude, λ , and SOC during the complete driving mission. The red lines and the dotted black line in the bottom figure are the limits on the SOC and the reference SOC, respectively.

4. SIMULATION RESULTS

In this section, results from tests where the hybrid and non-hybrid vehicle were evaluated on the driving mission defined in Section 1.1 are presented. For both vehicles the reference speed to the cruise controller was constant and chosen separately, for each vehicle, to give an average speed of 80 km/h. The non-hybrid vehicle was loaded to a total mass of 40 tonnes and the hybrid vehicle was loaded with the same amount, with the addition of the estimated mass of the electrical drive system of 1000 kg, giving it a total mass of 41 tonnes.

From Fig. 6 it can be observed that the control strategy for the hybrid vehicle keeps the SOC within its limits, fluctuating around the desired SOC. The final SOC is higher than the initial SOC making it possible to directly compare the results between the hybrid and the non-hybrid vehicle. Ideally the final SOC should be the same as the initial SOC since this would give the best fuel economy. However, the fact that the driving mission ends with two long downhills makes it hard to achieve this with the current control strategy, and instead some type of look-ahead control would probably be necessary.

In Fig. 7 some signals from a segment of the driving mission is shown. The segment starts with a downhill, where the non-hybrid vehicle uses the friction brake to slow down the vehicle while the hybrid vehicle turn off the engine and use regenerative braking to charge the battery.

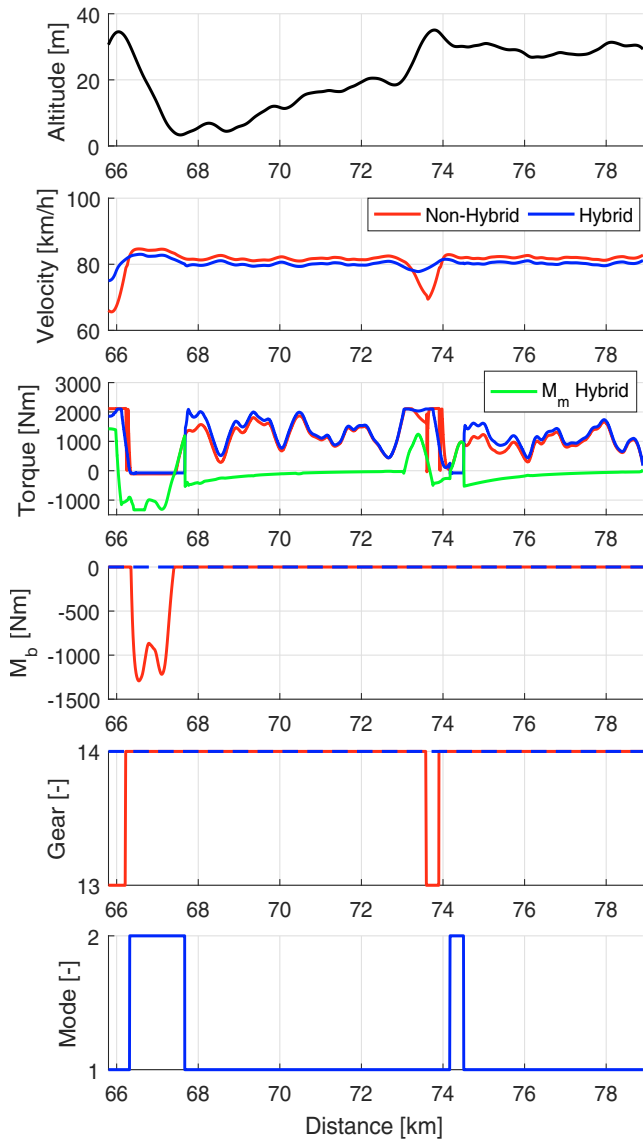


Fig. 7. Altitude, velocity, engine torque, M_e , motor torque, M_m , friction brake torque, M_{fr} , gear, and hybrid mode for a segment of the driving mission.

The energy recovered during braking is then used in the steepest part of the uphill, where the non-hybrid vehicle loses speed and has to change gear, while the hybrid lets the motor assist the engine and in this way avoids changing gear.

The effect the two control strategies have on the exhaust system can be seen in Fig. 8, where some signals related to the temperature in the exhaust system for the same segment of the driving mission as in Fig. 7 are shown. One can see that when the non-hybrid vehicle uses the friction brakes to slow down the vehicle, with the engine still spinning and pumping cold air through the exhaust system, the temperature in the SCR catalyst falls quickly. For the hybrid vehicle, which instead uses regenerative braking with the engine turned off, the temperature in the SCR catalyst is almost constant during braking, there is only a small temperature drop caused by thermal conduction and convection to the surrounding air.

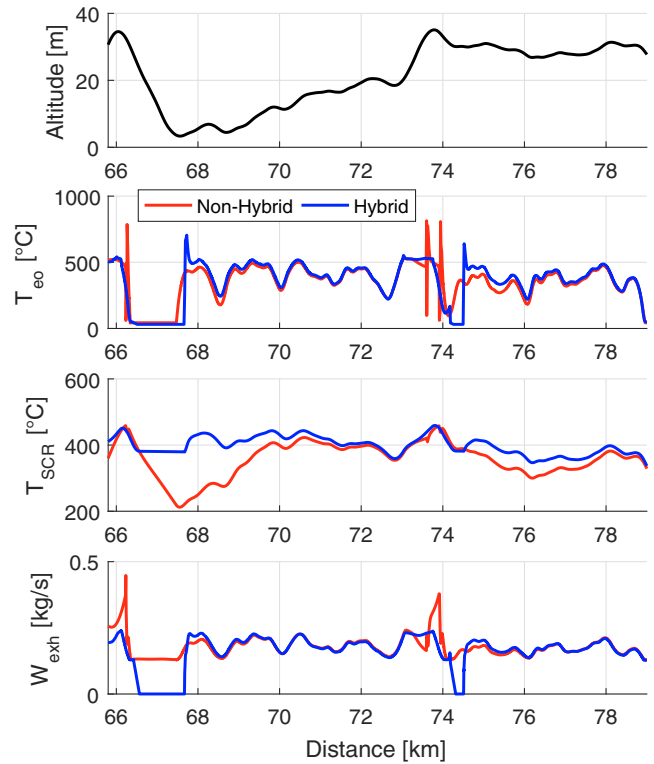


Fig. 8. Altitude, engine-out exhaust temperature, T_{eo} , SCR catalyst temperature, T_{SCR} , and exhaust mass flow, W_{exh} , for a segment of the driving mission. The spikes in T_{eo} at the beginning and middle of the plot are related to gear changes.

Fig. 9 shows the distribution of exhaust gas mass of different temperatures entering the SCR catalyst. One can see that the temperatures of the exhaust gas entering the SCR catalyst are higher for the hybrid vehicle than for the non-hybrid vehicle, in particular, there is a big difference for temperatures below 200 °C. This leads to higher temperatures in the SCR catalyst for the hybrid, which can be verified in Fig. 10, where the temperature of the SCR catalyst is shown over the complete driving mission. One can see that the temperature of the SCR catalyst for the hybrid vehicle most often lies between 300 °C and 500 °C, which is the most effective temperature range of the catalyst Winkler et al. (2003), while for the non-hybrid the temperature more often goes below this temperature range. This means that the conversion rate of NO_x is higher for the hybrid vehicle, which is verified in Table 1, where it can be seen that the conversion rate is 6 % higher for the hybrid vehicle compared to the non-hybrid vehicle. One can also see that the engine-out NO_x is lower for the hybrid vehicle, the reason for this is that some of the work needed to perform the driving mission is done by the motor instead of the engine and, also, the motor is some times used to shift the operating point of the engine towards an operating point where less NO_x is produced. Together, the higher conversion rate and lower engine-out NO_x lead to 31 % lower tail-pipe NO_x for the hybrid vehicle compared to the non-hybrid vehicle. Here it should also be mentioned that the urea dosing controller is quite simple and more advanced strategies could probably be used to improve the conversion rate for both vehicles.

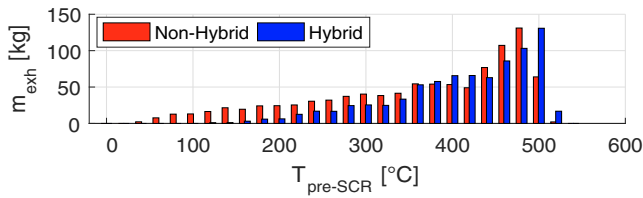


Fig. 9. Distribution of exhaust gas mass entering the SCR catalyst with different temperatures.

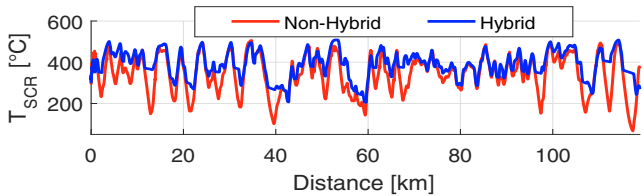


Fig. 10. Temperature of the SCR catalyst for both vehicles during the driving mission.

Table 1. Emissions and fuel consumption for both vehicles.

Quantity	Non-Hybrid	Hybrid
$\text{NO}_{x,co}$ [g]	706	635
$\text{NO}_{x,tp}$ [g]	132	91
$\text{NH}_{3,tp}$ [g]	6.63	10.4
NO_x conversion rate [%]	81	86
Fuel consumption [L/10km]	3.69	3.55
AdBlue consumption [L/10km]	0.287	0.276

Finally, Table 1 also shows that the fuel consumption is 3.8 % lower for the hybrid vehicle compared to the non-hybrid vehicle. Here it should be pointed out that, as mentioned earlier, the final SOC of the hybrid vehicle is higher than its initial SOC, which means that some fuel has been used to charge the battery. Also, the driving mission consists only of highway driving without any stops or larger variations in speed, this almost completely limits the use of regenerative braking to parts where there is downhill. Therefore, larger improvements in fuel economy can be expected on driving missions that are better suited for hybrid vehicles.

5. CONCLUSION

The benefits of hybridization of long haulage trucks are investigated by designing and evaluating a control strategy for a hybrid electric long haulage truck against a conventional, non-hybrid, vehicle. It was shown that the hybridization gave new capabilities to control the temperatures in the exhaust aftertreatment system, making it possible to increase its efficiency. In a specific case the hybridization lead to 31 % lower NO_x emissions and an improvement in fuel economy of 3.8 %.

REFERENCES

Brahma, A., Guezennec, Y., and Rizzoni, G. (2000). Optimal energy management in series hybrid electric vehicles. In *American Control Conference, 2000. Proceedings of the 2000*, volume 1. IEEE.

CARB (2015). Draft technology assessment: Heavy-duty hybrid vehicles. Technical report, California Environmental Protection Agency Air Resources Board.

Chan, C.C. (2007). The state of the art of electric, hybrid, and fuel cell vehicles. *Proceedings of the IEEE*, 95(4).

Eriksson, L. (2001). Simulation of a vehicle in longitudinal motion with clutch lock and clutch release. *3rd IFAC Workshop Advances in Automotive Control Preprints*.

Eriksson, L., Larsson, A., and Thomasson, A. (2016). The aac2016 benchmark-look-ahead control of heavy duty trucks on open roads. *IFAC-PapersOnLine*, 49(11).

Foster, D., Cloudt, R., and Willems, F. (2008). Towards integrated powertrain control: exploiting synergy between a diesel hybrid and aftertreatment system in a distribution truck. In *Intelligent Vehicles Symposium, 2008 IEEE*.

Hellström, E., Åslund, J., and Nielsen, L. (2010). Management of kinetic and electric energy in heavy trucks. *SAE International Journal of Engines*, 3(2010-01-1314).

Le Berr, F., Abdelli, A., Postariu, D.M., and Benlamine, R. (2012). Design and optimization of future hybrid and electric propulsion systems: An advanced tool integrated in a complete workflow to study electric devices. *Oil & Gas Science and Technology—Revue d'IFP Energies nouvelles*, 67(4).

Lescot, J., Sciarretta, A., Chamailard, Y., and Charlet, A. (2010). On the integration of optimal energy management and thermal management of hybrid electric vehicles. In *Vehicle Power and Propulsion Conference (VPPC), 2010 IEEE*. IEEE.

Paganelli, G., Guerra, T., Delprat, S., Santin, J., Delhom, M., and Combes, E. (2000). Simulation and assessment of power control strategies for a parallel hybrid car. *Proceedings of the Institution of Mechanical Engineers, Part D: Journal of Automobile Engineering*, 214(7).

Sivertsson, M., Sundström, C., and Eriksson, L. (2011). Adaptive control of a hybrid powertrain with map-based ecms. *IFAC Proceedings Volumes*, 44(1).

Van Helden, R., Verbeek, R., Willems, F., and van der Welle, R. (2004). Optimization of urea scr denox systems for hd diesel engines. Technical report, SAE Technical Paper.

Wahlström, J. and Eriksson, L. (2011). Modelling diesel engines with a variable-geometry turbocharger and exhaust gas recirculation by optimization of model parameters for capturing non-linear system dynamics. *Proceedings of the Institution of Mechanical Engineers, Part D: Journal of Automobile Engineering*, 225(7).

Willems, F. and Foster, D. (2009). Integrated powertrain control to meet future co₂ and euro-6 emissions targets for a diesel hybrid with scr-deno x system. In *2009 American Control Conference*. IEEE.

Willems, F., Spronkmans, S., and Kessels, J. (2011). Integrated powertrain control to meet low co₂ emissions for a hybrid distribution truck with scr-deno x system. In *ASME 2011 Dynamic Systems and Control Conference and Bath/ASME Symposium on Fluid Power and Motion Control*. American Society of Mechanical Engineers.

Winkler, C., Flörchinger, P., Patil, M., Gieshoff, J., Spurk, P., and Pfeifer, M. (2003). Modeling of scr denox catalyst-looking at the impact of substrate attributes. Technical report, SAE Technical Paper.

XALT Energy (2016). Xalt 31 ah high power (hp) superior lithium ion cell. Available from: <http://www.xaltenergy.com>. [28 October 2016].